Journal of Applied Physics

First-principles calculations of physical properties and superconductivity of orthorhombic Mo_2BC and Nb_2BN

Cite as: J. Appl. Phys. **130**, 153902 (2021); https://doi.org/10.1063/5.0060200
Submitted: 16 June 2021 • Accepted: 01 October 2021 • Published Online: 15 October 2021

S. Saib, H. Y. Uzunok, Ertugˇrul Karaca, et al.

Journal of Applied Physics ARTICLE scitation.org/journal/jap

First-principles calculations of physical properties and superconductivity of orthorhombic Mo_2BC and Nb_2BN

Cite as: J. Appl. Phys. **130**, 153902 (2021); doi: 10.1063/5.0060200
Submitted: 16 June 2021 · Accepted: 1 October 2021 ·
Published Online: 15 October 2021

S. Saib,[1] H. Y. Uzunok,[2,a)] Ertuğrul Karaca,[3] S. Bağcı,[2] H. M. Tütüncü,[2] and G. P. Srivastava[4]

AFFILIATIONS

[1]Laboratory of Materials Physics and Its Applications, University of M'sila, 28000 M'sila, Algeria
[2]Fen-Edebiyat Fakültesi, Fizik Bölümü, Sakarya Üniversitesi, 54050 Sakarya, Turkey
[3]BIMAYAM Biyomedikal, Manyetik ve Yarıiletken Malzemeler Araştırma Merkezi, Sakarya Üniversitesi, 54050 Sakarya, Turkey
[4]School of Physics, University of Exeter, Stocker Road, Exeter EX4 4QL, United Kingdom

[a)]**Author to whom correspondence should be addressed:** hyuzunok@sakarya.edu.tr

ABSTRACT

Ab initio pseudopotential calculations have made for the structural, electronic, elastic, mechanical, and electron–phonon interaction properties of molybdenum borocarbide (Mo_2BC) and niobium boronitride (Nb_2BN) superconductors. Analysis of the structural and electronic properties reveals that the nature of bonding in both these compounds is a combination of covalent, ionic, and metallic. The near-Fermi electronic states in both compounds are occupied by the d states of transition metal atoms. The electronic density of states at the Fermi level in Mo_2BC is significantly higher than that in Nb_2BN. Lattice dynamical calculations verify their dynamical stability in the base-centered orthorhombic Mo_2BC-type crystal structure. We find that the total electron–phonon coupling constant is equal to 0.745 for Mo_2BC and 0.539 for Nb_2BN. The calculated superconducting transition temperature of 7.41 K for Mo_2BC and 3.50 K for Nb_2BN is comparable with their experimental values of 7.2 and 4.4 K, respectively.

I. INTRODUCTION

Transition metal carbides, nitrides, and borides have received a great deal of attention because they are chemically inert, refractory, and stiff substances with high thermal and electrical conductivitives.[1–7] Such materials have been greatly utilized as cutting tools and for wear-resistant coatings.[8–15] Also, it is well known that in numerous binary and ternary carbides and nitrides, the availability of a common subcell formed by six transition metal atoms at the corners of an octahedron with carbon and nitrogen is suitable for the formation of the superconducting state.[16–27]

Molybdenum borocarbide (Mo_2BC) is special since it is one of the few purely ternary compounds including atoms of transition metal, carbon, and boron. The crystal structure of this compound is related to those in the binary system by a common Mo_6C octahedral subcell. Indeed, this compound shows superconducting behavior with a superconducting transition temperature ranging from 5.0 to 7.5 K.[21,22] Polycrystalline sample, synthesized by the arc-melting method from commercially existing Mo_2B powder precursor, was reported to have a superconducting transition temperature of around 7.2 K.[27] In 2014, niobium boronitride (Nb_2BN),[26] being isostructural with Mo_2BC, has also been reported to show superconductivity at around 4.4 K.[26] Before this experimental study,[26] the superconducting transition temperature of this compound was reported to be 2.5 K.[28]

Ab initio calculations[29,30] reveal that Mo_2BC displays a matchless combination of high hardness and moderate ductility due to its large Young's modulus and considerably positive Cauchy pressure. This result is very interesting because although conventional superconductors meet the problem of low stiffness, which withholds them from a wide range of applications. In view of this, high mechanical stiffness in combination with moderate ductility makes Mo_2BC a hopeful candidate for the protection of cutting and forming tools. Emmerlich *et al.*[29] have studied the electronic properties of this superconductor by employing the density functional theory within its generalized gradient approximation (GGA).

According to this *ab initio* calculation, the electronic states in the vicinity of the Fermi level mainly consist of Mo 4d states. This work also finds that the molybdenum carbide bonds are stronger than the molybdenum boride bonds. Following this work, projector-augmented-wave (PAW) potentials and the GGA[30] have been utilized to examine the electronic and elastic properties of X_2BC X = Ti, V, Zr, Nb, Mo, Hf, Ta, and W. According to this theoretical study, all the studied compounds display high hardness, which renders these compounds as encouraging candidates for protection of cutting and forming tools. The full-potential linearized augmented plane wave method with the GGA[31] has been used to analyze the mechanical and electronic properties of Nb_2BN in comparison with the corresponding results for Mo_2BC. This *ab initio* work reveals that the essential contribution to the electronic density of states at the Fermi level for both superconductors is realized by the d states of their transition metal atoms, which is in agreement with previous theoretical calculations.[29,30]

While the electronic and elastic properties of Mo_2BC and Nb_2BN have been presented and discussed in detail,[29–31] their lattice dynamical properties have been completely ignored in the literature. It is well known that explanation of several physical properties, such as electrical and thermal resistivity, thermal expansion, and superconductivity, requires the knowledge of phonons and their interactions with electrons. In this work, we analyze the structural and electronic properties of both superconductors by conducting *ab initio* pseudopotential calculations within the GGA.[32,33] The calculation of single crystal elastic constants for both investigated compounds have been executed by using the strain-stress method.[34] The isotropic bulk modulus, the isotropic shear modulus, Poisson's ratio, and Young's modulus have been achieved with the assistance of the Voigt–Reuss–Hill (VRH) scheme.[35–38] Lattice dynamical calculations have been realized by using the density functional perturbation theory in the linear response approach.[32,33] After phonon calculations, we have conducted *ab initio* linear response calculations of electron–phonon interaction matrix elements for both studied compounds. Their Eliashberg spectral functions have been integrated to attain the average electron–phonon coupling parameter and the logarithmic average of phonon frequency for them. Finally, inserting these results into the Allen–Dynes modified McMillan equation,[39–41] the superconducting transition temperatures for the studied compounds are evaluated and compared with the reported experimental values.[26,27]

II. METHOD

The corresponding first-principles calculations have been executed utilizing the Quantum-Espresso *ab initio* simulation package,[32,33] which is an implementation of the pseudopotential plane-wave method based on the density functional theory. Kohn–Sham equations[42] have been solved making use of Perdew–Burke–Ernzerhof generalized gradient approximation.[43] The ultrasoft pseudopotentials of Vanderbilt type[44] are employed to represent the Coulomb interactions between valence electrons and ionic cores, while the structural optimization has been achieved by utilizing the Broyden–Fletcher–Goldfrab–Shanno optimized method.[45] An energy cutoff limiting the number of plane waves in the basis set is set to 60 Ry for both compounds considered in this work. The Brillouin zone integrations have been conducted by using Monkhorst–Pack grids[46] of $(9 \times 9 \times 9)$ and $(27 \times 27 \times 27)$ for structural and electronic calculations, respectively.

Phonon calculations have been conducted by using the linear response method.[32,33] Within this scheme, second order derivatives of the total energy have been calculated to determine the dynamical matrix. A static linear response of the valence electrons is considered in terms of the variation of the external potential corresponding to periodic displacements of the atoms in the unit cell. The screening of the electronic system in response to the displacement of the atoms is taken into account in a self-consistent manner. Since phonon calculations are computationally very time consuming, we have first calculated 8 and 21 dynamical matrices on the $(3 \times 3 \times 3)$ $\boldsymbol{q}$-point and $\boldsymbol{q}(4 \times 4 \times 4)$ $\boldsymbol{q}$-point meshes, respectively.[46] Then, Fourier-transformed these dynamical matrices into real space to extract the force constants, which are used to calculate phonon frequencies for any $\boldsymbol{q}$-points.

The electron–phonon interaction calculations have been performed by combining the linear response theory[32,33] and the Migdal–Eliashberg theory.[47,48] First, the calculation of electron–phonon matrix elements ($g^{\mathbf{qj}}_{(\mathbf{k}+\mathbf{q})m;\mathbf{k}n}$) has been executed with the help of linear response theory.[32,33] These matrix elements are used to treat the scattering of electron in state $|\mathbf{k}n>$ to state $|\mathbf{k}+\mathbf{q}m>$ due to perturbation originating out of the phonon mode $\omega_{\mathbf{qj}}$. With this, we are able to obtain the phonon linewidth $\gamma_{\mathbf{qj}}$,

$$\gamma_{\mathbf{qj}} = 2\pi\omega_{\mathbf{qj}} \sum_{\mathbf{k}nm} |g^{\mathbf{qj}}_{(\mathbf{k}+\mathbf{q})m;\mathbf{k}n}|^2 \delta(\varepsilon_{\mathbf{k}n} - \varepsilon_F)\delta(\varepsilon_{(\mathbf{k}+\mathbf{q})m} - \varepsilon_F). \quad (1)$$

Then, the electronic density of states, phonon density of states, and electron–phonon matrix elements can be utilized to get the Eliashberg spectral function $[\alpha^2 F(\omega)]$ from the following expression:

$$\alpha^2 F(\omega) = \frac{1}{2\pi N(E_F)} \sum_{\mathbf{qj}} \frac{\gamma_{\mathbf{qj}}}{\hbar\omega_{\mathbf{qj}}} \delta(\omega - \omega_{\mathbf{qj}}), \quad (2)$$

where $N(E_F)$ represents the electronic density of states at the Fermi level. Having obtained the Eliashberg spectral function, the values of average electron–phonon coupling constant λ and logarithmically averaged phonon frequency $\omega_{\ln}$ can be derived from its integration with the following expressions:

$$\lambda = \int_0^\infty \frac{\alpha^2 F(\omega)}{\omega}\, d\omega, \quad (3)$$

$$\omega_{ln} = exp\left(2\lambda^{-1} \int_0^\infty \frac{d\omega}{\omega} \alpha^2 F(\omega) ln\omega\right). \quad (4)$$

Thus, the superconducting transition temperature can be estimated by inserting the values of λ and $\omega_{\ln}$ into the Allen–Dynes modified McMillan equation,[39–41]

$$T_c = \frac{\omega_{\ln}}{1.2} \exp\left(-\frac{1.04(1+\lambda)}{\lambda - \mu^*(1+0.62\lambda)}\right), \quad (5)$$

where μ^* represents the screening Coulomb pseudopotential, frequently taking a typical value between 0.10 and 0.20.[39–41,49] Following the experimental works on Mo_2BC and Nb_2BN superconductors,[26,27] its value is chosen to be 0.13. Finally, the values of the average electron–phonon coupling parameter and the density of states at the Fermi level can be used to calculate the specific heat coefficient (γ) at low temperatures with the following approximate formula:[50]

$$\gamma = \frac{\pi^2}{3} n N_o k_B^2 N(E_F)(1+\lambda), \tag{6}$$

where n, N_o, and k_B refer to the number of atoms per formula unit, the Avogadro number, and the Boltzmann constant, respectively.

III. RESULTS

A. Structural and electronic properties

Both compounds, M_2BX (M = Mo or Nb, X = C or N), crystallize in the base-centered orthorhombic Mo_2BC-type crystal structure with space group no. 63 (C_{mcm}) and two formula units per primitive cell. The atomic positions inside a primitive unit cell can be categorized as four nonequivalent crystallographic sites: M_1, M_2, B, and X according to symmetry. The atoms occupy the following Wyckoff positions: two M_1 atoms in the position 4c (0, y_{M_1}, 0.25), two M_2 atoms in the position 4c (0, y_{M_2}, 0.25), two B atoms in the position (4c) (0, y_B, 0.25), and two X atoms in the position (4c) (0, y_X, 0.25). Here, y_{M_1}, y_{M_2}, y_B, and y_X represent the inner coordinates for the related atoms. Therefore, the crystal structure is characterized by three lattice parameters (*a*, *b*, and *c*) and four inner coordinates (y_{M_1}, y_{M_2}, y_B, and y_X).

The bulk modulus and its pressure derivative have been determined using the Murnaghan equation of states.[51] The calculated values of three lattice parameters, four inner coordinates, bulk modulus, and its pressure derivative are listed in Table I, together with available experimental data[22–24,26,27,29] and previous theoretical results.[29–31] From Table I, it can be noted that the average deviation of our results relative to experimental results for the lattice parameters of both superconductors is close to 1%, while the calculated values of inner coordinates for both compounds are almost equal to their experimental values.[22,26] Our calculated value of bulk modulus for Mo_2BC (317.3 GPa) is almost equal to the previous GGA value of 313 GPa.[30] It is worth mentioning that our calculated value lies between that of TiN (295 GPa)[52] and that of cubic BN (376 GPa),[53] suggesting a considerably stiff material. Furthermore, the bulk modulus values of both compounds are larger than several other carbides, such as TiC (225 GPa), HfC (238 GPa), and VC (281 GPa).[54]

Using the calculated structural parameters, the base-centered orthorhombic crystal structure of Mo_2BC (Nb_2BN) is sketched in Fig. 1(a), and the coordination numbers of Mo (Nb), B, and C(N) atoms are displayed in Fig. 1(b). The crystal structure contains carbon-centered transition-metal-atom octahedra. There are four types of chemical bonds in these compounds: Mo–Mo, Mo–B, Mo–C, and B–B, with no evidence of direct B–C and C–C bonds. According to Fig. 1(b), the coordination numbers of Mo1, Mo2, B, and C atoms are 13, 9, 8, and 6, respectively. Each Mo1 atom has two Mo1 neighbors with a shorter distance of 2.950 Å and four Mo2 neighbors at a slightly longer distance of 2.951 Å. These distances are slightly longer than that in the body-centered cubic molybdenum, where each molybdenum atom has eight neighbors at 2.725 Å. It is worth mentioning that the Mo–Mo bond in Mo_2BC is metallic, being unfavorable for hardness. Each Mo1 atom has six nearest boron neighbors at 2.314 Å, which is shorter than the sum of the covalent radii of 2.41 Å for molybdenum and boron atoms. These observations imply that these atoms are bonded by a mixture of ionic and covalent interactions. However, Mo2 atoms do not interact with boron atoms, but each Mo2 atom has five nearest carbon neighbors at 2.183 Å, being considerably shorter than the sum of the covalent radii of 2.31 Å for molybdenum and carbon atoms. Furthermore, the Mo1–C distance of 2.085 Å is also considerably smaller than this sum. This result signals a strong covalent interaction between molybdenum and carbon atoms. Furthermore, each B atom has two nearest boron neighbors at 1.817 Å, which is close to the sum of the covalent radii of 1.70 Å for boron atoms. Taken together, we can say that chemical bonding

TABLE I. The calculated values of lattice parameters (*a*, *b*, and *c*), inner coordinates (y_{M1}, y_{M2}, y_B, and y_X), bulk modulus (*B*), and its pressure derivative (B') for superconductors Mo_2BC and Nb_2BN and their comparison with the corresponding experimental data and the corresponding previous theoretical results.

Compound	*a* (Å)	*b* (Å)	*c* (Å)	(y_{M1}, y_{M2})	(y_B, y_X)	*B* (GPa)	B'
Mo_2BC	3.104	17.501	3.065	(0.0720, 0.3144)	(0.4721, 0.1911)	317.3	3.25
Experimental[22,23]	3.086	17.350	3.047	(0.7210, 0.3139)	(0.4731, 0.192)		
Experimental[24]	3.088	17.348	3.046				
Experimental[29]	3.089	17.325	3.044				
Experimental[27]	3.086	17.343	3.047				
GGA[29]	3.094	17.768	3.091				
GGA[30]	3.119	17.580	3.082			313	
GGA[31]	3.114	17.502	3.065	(0.0717, 0.3145)	(0.4719, 0.1912)		
Nb_2BN	3.172	17.952	3.120	(0.0728, 0.3180)	(0.4730, 0.1941)	285.2	2.00
Experimental[26]	3.170	17.850	3.110	(0.0721, 0.3139)	(0.4731, 0.1920)		
Experimental[28]	3.172	17.841	3.114				
GGA[31]	3.172	17.975	3.125	(0.0728, 0.3184)	(0.4730, 0.1941)		

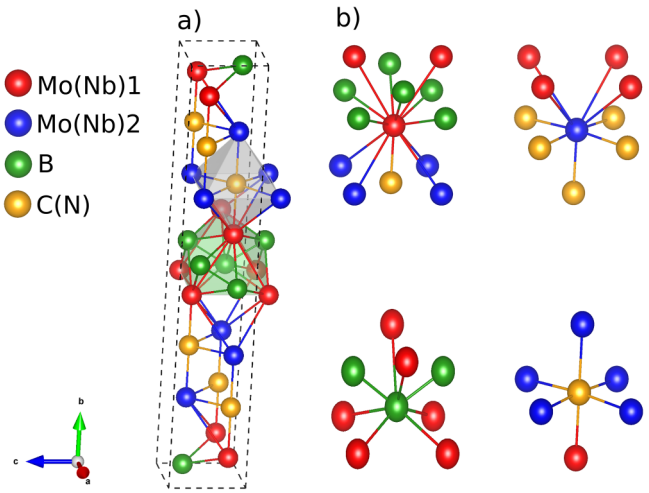

FIG. 1. (a) Three-dimensional view of the base-centered orthorhombic crystal structure of Mo_2BC and Nb_2BN. (b) Coordination numbers of Mo (Nb), B, and C (N) atoms.

in Mo_2BC is a combination of covalent, ionic, and metallic in nature. We have made the same observations for Nb_2BN.

The energy-band dispersion of Mo_2BC along the principal symmetry axes in the Brillouin zone of base-centered orthorhombic lattice is shown in Fig. 2(a). The energy zero is taken at the Fermi level. The overall features of the band profile in this calculation are similar to those presented by previous GGA calculations.[29,30] The distinct crossover behavior between the valence and the conduction bands reveals that Mo_2BC is metallic. In order to determine the additives of different atoms and orbitals and the nature of chemical bonding in Mo_2BC, its total density of states (DOS) and partial density of states diagrams are depicted in Fig. 2(b). The most prominent region of electronic DOS with strong peaks for the chemical bonding extends from −8 to −2 eV since the d states of molybdenum atoms interact strongly with the p states of nonmetal atoms. In particular, the strongest DOS peak at −5.3 eV is mainly formed by a high degree hybridization of Mo2 4d states with C 2p states. This strong hybridization is expected since each second molybdenum (Mo2) atom has five nearest carbon neighbors, but each first molybdenum (Mo1) atom has only one carbon contact. This hybridization is clear evidence of strong covalent interaction between the related atoms. In addition to this strongest peak, there is another peak at −3.8 eV, resulting from a considerable hybridization of Mo1 4d states with B 2p states and smaller contributions from Mo2 4d and C 2p states. This hybridization can be linked to the six nearest boron neighbors of each first molybdenum (Mo1) atom. This hybridization confirms that the related atoms are bonded not only by ionic interaction but also by significantly covalent interaction. As can be seen from Fig. 2(b), the main orbital occupancy near the Fermi level arises from the d electrons of molybdenum atoms, which is therefore responsible for the metallic behavior. Altogether, the electronic DOS for Mo_2BC confirms that the bonding in this compound can be classified as an interplay

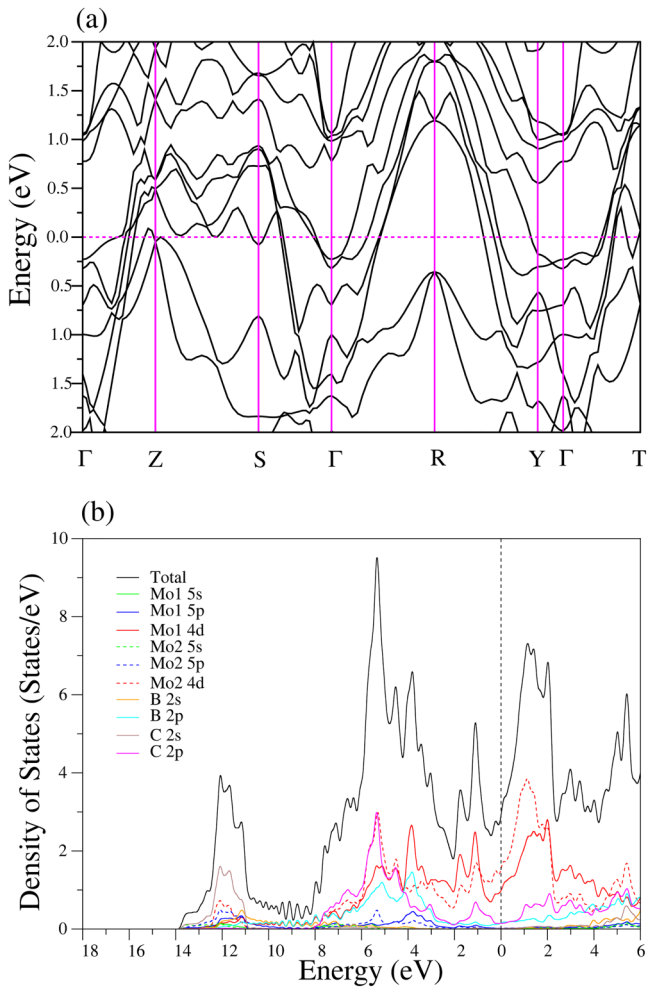

FIG. 2. (a) The calculated electronic band structure of Mo_2BC along the most important axes of symmetry in the Brillouin zone of base-centered orthorhombic lattice. The Fermi level is set to 0 eV. (b) Total and partial electronic density of states for Mo_2BC.

between covalent, metallic, and ionic characters. It is well known that in many binary and ternary carbides and nitrides, the existence of a common subcell formed by six transition metal atoms of an octahedron with carbon or nitrogen atoms in the center is favorable for the occurrence of the superconducting state. The implications of the above covalent bonds are crucial for the superconductor Mo_2BC, in which Cooper pairs can be coupled through phonons.

Since electrons close to the Fermi level have a potential to form Cooper pairs, the electronic density of states at the Fermi level [$N(E_F)$] is one of the important key quantities to examine the origin of superconductivity in metallic materials. For Mo_2BC, the DOS at the Fermi level, $N(E_F)$, amounts to 2.909 states/eV, a result that accords very well with the previous GGA values of 3.060[27] and 2.872 states/eV.[31] This value is composed of roughly 35% from

Mo1 electronic states, 54% from Mo2 electronic states, 5% from B electronic states, and 6% from C electronic states. Thus, in the light of BCS theory, we can suggest that the d electrons of second molybdenum (Mo2) atoms are more strongly involved in the formation of a superconducting state for Mo_2BC.

The energy-band dispersion of Nb_2BN along the principal symmetry axes in the Brillouin zone of base-centered orthorhombic lattice is displayed in Fig. 3(a). Nb_2BN also exhibits a metallic feature with some bands crossing the Fermi level. The total density of states and partial density of states are shown in Fig. 3(b). Different from the valence DOS of Mo_2BC, the valence DOS of Nb_2BN can be divided into two apparent parts with a gap of 3.4 eV: the lower one spreading from −16.6 to −14.80 eV and the upper one lengthening from −11.4 to the Fermi level. The lower part of the valence DOS region is mainly contributed by N 2s states with much smaller contributions from Nb2 4d and Nb2 5p states. The DOS features between −11.4 and −8.0 eV are shaped by a mixture of B 2s, Nb1 5p, and Nb1 4d states. The DOS region between −8.0 and −2.0 eV contains several apparent DOS peaks. In particular, the partial DOS profiles for both N 2p and Nb2 4d states are similar in the energy range from −8.0 to −5.0 eV, signaling considerable hybridization between these two states. Once again, the main orbital occupancy near the Fermi level comes from the 4d electrons of transition metal atoms, which are the principal reason for the metallicity. The value of $N(E_F)$ for Nb_2BN is calculated to be 2.325, being in agreement with a previous GGA value of 2.302 states/eV.[31] Approximately 43%, 43%, 5%, and 9% of this value is contributed by the Nb1, Nb2, B, and N electronic states, respectively. For this compound, different from Mo_2BC, the contribution from the d states of first transition metal atoms (Nb1) is almost equal to that of second transition metal atoms (Nb2). The value of $N(E_F)$ for Nb_2BN is considerably lower than that for Mo_2BC. This lower $N(E_F)$ value must be a good reason why its T_c value is lower than that of Mo_2BC, since the electron–phonon coupling parameter (λ) depends linearly on the value of $N(E_F)$ according to the well-known McMillan–Hopfield expression, which is given by the following equation:[39]

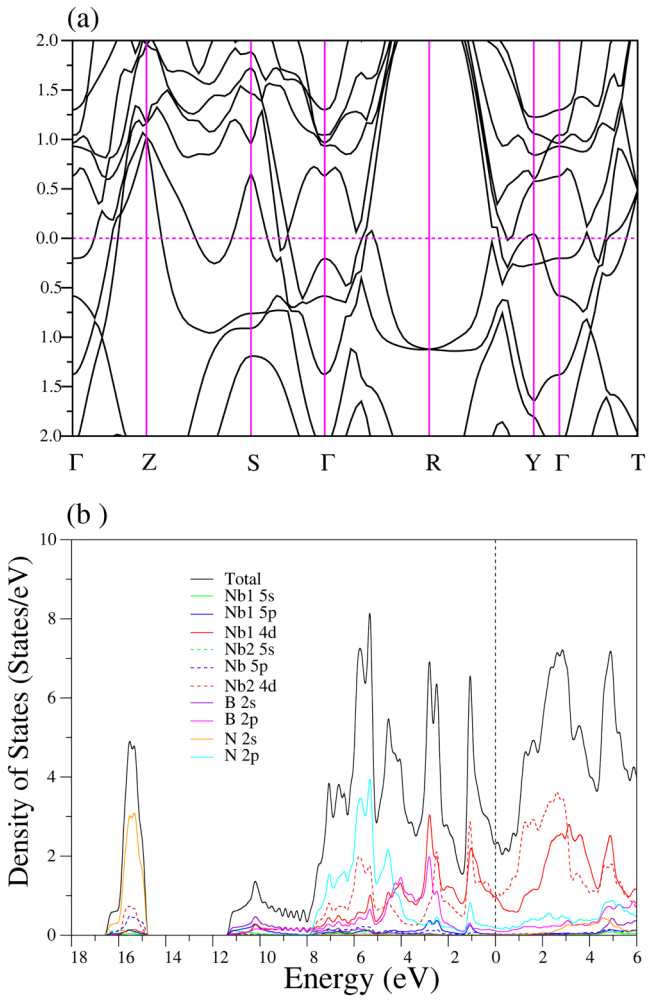

FIG. 3. (a) The calculated electronic band structure of Nb_2BN along the most important axes of symmetry in the Brillouin zone of base-centered orthorhombic lattice. The Fermi level is set to 0 eV. (b) Total and partial electronic density of states for Nb_2BN.

$$\lambda = \frac{N(E_F) < I^2 >}{M < \omega^2 >}, \tag{7}$$

where $< \omega^2 >$, $< I^2 >$, and M represent the averaged square of the phonon frequency, the averaged square of the electron–phonon matrix element, and the mass involved, respectively. Examination of the electronic density of states for both studied superconductors reveals that the Cooper pairs in them are substantially formed by the d electrons of transition metal atoms. However, a sound statement of considerable T_c difference between the two investigated superconductors still requires calculations of their phonon and electron–phonon interaction properties in order to identify which phonon vibrations are strongly involved in the process of scattering of electrons.

The high-symmetry points of base-centered orthorhombic structure and the calculated Fermi surface (FS) sheets of Mo_2BC and Nb_2BN are presented in Fig. 4 (obtained by using the XCrySDen software[55]). Results for Mo_2BC and Nb_2BN are shown in columns (a) and (b), respectively. For both compounds, there are no closed surfaces occurring around the Γ point. Using Fig. 2(a), we can deduce that all the Fermi crossing bands in Mo_2BC have both hole and electron pocket features. All FS sheets, except for the first band, have a chimney-like feature along the Γ-S direction. The last FS shows nesting features along the Γ-Z direction, which could affect the electron–phonon interaction and enhance its value for the Mo_2BC compound. On the contrary, the Nb_2BN compound's FS has no significant nesting features and distinctly has different features from Mo_2BC. We can say that both electrons and holes can transport charge in both compounds and thus could lead to multi-band superconductivity.

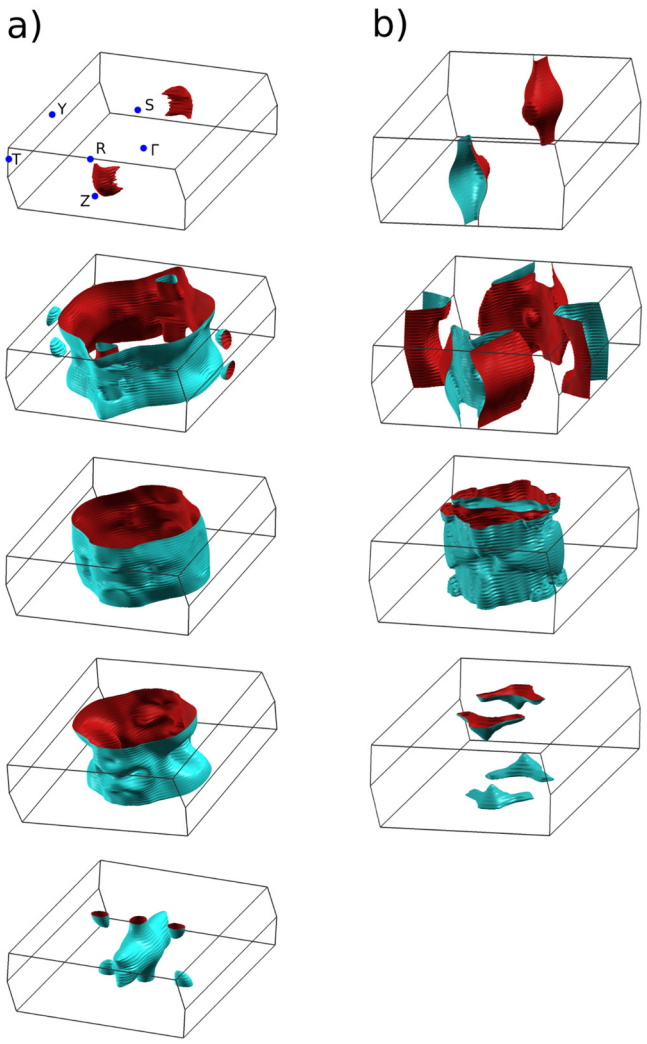

FIG. 4. The calculated Fermi surface sheets of (a) Mo_2BC and (b) Nb_2BN. Each color corresponds to the different spin of an electron in an electronic energy band. Mo_2BC has five Fermi surface sheets that can be seen on the right column, and Nb_2BN has four Fermi surface sheets placed on the left column. The high-symmetry points of base-centered orthorhombic structure shown in the first Fermi surface of Mo_2BC.

B. Elastic and mechanical properties

Investigation of elastic constants and elastic moduli is necessary for realizing macroscopic mechanical properties of solids and for the design of hard materials and their potential technological applications. We have calculated the zero-pressure second order elastic constants C_{ij} by using the strain-stress method.[34] A small finite strain is applied to the optimized structure and the atomic positions are fully optimized. Then, the elastic constants of both studied compounds are determined from the stress of the strained structure. The calculated values of single crystal elastic constants are listed in Table II, along with other theoretical results[29,31] for comparison. Although no experimental investigations have been conducted to measure the independent elastic constants of both studied superconductors, our GGA results are found to be comparable with previous theoretical results.[29,31] For both compounds, C_{33} is higher than the other elastic constants, revealing that they are very incompressible under uniaxial stress along the z axis. We mention that C_{11}, C_{22}, and C_{33} correspond to the linear compression along the crystal axis, while C_{44}, C_{55}, and C_{66} are associated with shear deformation. Therefore, both investigated compounds exhibit stronger resistance to the unidirectional compression than the shear deformation because the values of C_{11}, C_{22}, and C_{33} are significantly higher than the corresponding values of C_{44}, C_{55}, and C_{66}. It is well known that the elastic stability is a required condition for a stable crystal. For the mechanical stability of orthorhombic crystal, the following conditions[38] regarding elastic constants have to be obeyed:

$$C_{ii} > 0 \ (i = 1, 6), \quad C_{11} + C_{22} - 2C_{12} > 0,$$

$$C_{22} + C_{33} - 2C_{23} > 0, \quad C_{11} + C_{33} - 2C_{13} > 0,$$

$$C_{11} + C_{22} + C_{33} + 2C_{12} + 2C_{13} + 2C_{23} > 0.$$

As can be deducted from Table II, the above conditions are clearly satisfied for orthorhombic stability, indicating that both studied superconductors are mechanically stable in their crystal structures.

In this study, elastic moduli such as bulk modulus (B), shear modulus (G), Young's modulus (E), and Poisson's ratio (σ) have been obtained from the second order elastic constants with the well-known Voigt–Reuss–Hill approximation.[35–38] The calculated values of these quantities for both investigated compounds are listed in Table III, together with the measured value of Young's modulus for Mo_2BC[29] and previous GGA results.[29–31] In general, the calculated values in this work for both investigated superconductors are consistent with the previously available GGA results.[29–31] In particular, the calculated value of Young's modulus for Mo_2BC amounts to 456.98 GPa, which is slightly lower than its measured value of 460 GPa.[29] The calculated bulk moduli of both compounds accord very well with those directly determined from the fitting of the Murnaghan equation of states presented in Table I, signaling good accuracy of our elastic calculations. Results in Table III reveal that the shear moduli values of Mo_2BC are almost equal to those of Nb_2BN. However, the calculated results indicate that the values of bulk modulus and Young's modulus for Mo_2BC are higher than those for Nb_2BN, implying that Mo_2BC is harder than Nb_2BN.

The resistance of a compound to volume and shape change can be defined by bulk modulus and shear modulus, respectively. Table III reveals that the value of shear modulus is considerably lower than that of bulk modulus for both investigated compounds, implying that the shape deformation is much easier to appear than the volume change for them. The ratio between the bulk and the shear modulus B_H/G_H is utilized to estimate the brittle or ductile behavior of compounds. According to the Pugh criterion,[56] the ductile behavior is observed when this ratio is greater than 1.75

TABLE II. The calculated of second order elastic constants (in GPa) for orthorhombic superconductors Mo_2BC and Nb_2BN. Previous theoretical results are also included for comparison.

Compound	C_{11}	C_{12}	C_{13}	C_{22}	C_{23}	C_{33}	C_{44}	C_{55}	C_{66}
Mo_2BC	501.50	211.47	228.73	538.95	186.42	547.61	170.13	255.06	178.55
GGA[29]	551	221	204	566	210	553	168	241	182
GGA[31]	523.0	214.4	221.0	640.3	206.6	559.1	176.8	277.7	187.9
Nb_2BN	498.86	162.93	182.69	518.76	156.90	534.27	154.31	263.09	156.36
GGA[31]	485.1	156.2	194.6	564.3	139.6	513.4	174.4	207.0	187.9

or else the compound is brittle. The results presented in Table III suggest that Mo_2BC is moderately inclined to ductility and Nb_2BN is significantly inclined to brittleness. Poisson's ratio is also used to predict the brittle or ductile behavior of compounds. The ductile behavior is predicted when this ratio is greater than the limit value of 0.26 or else the compound is brittle.[57] This criterion also confirms that Mo_2BC is moderately prone to ductility and Nb_2BN is prone to brittleness. It is worth mentioning that a similar observation for Mo_2BC has been made in the previous GGA work of Emmerlich *et al.*[29]

C. Phonon and electron–phonon interaction properties

Group theory predicts the following irreducible representations of the optical phonon modes for these compounds corresponding to the point group symmetry D_{2h} (mmm):

$$\Gamma(D_{2h}(mmm)) = 4A_g + 4B_{1g} + 4B_{2g} + 3B_{1u} + 3B_{2u} + 3B_{3u}, \quad (8)$$

with all of them being singly degenerate. Frequencies and electron–phonon coupling parameters of zone-center phonon modes and the dominant atomic contributions to their eigenvectors are presented in Tables IV and V for Mo_2BC and Nb_2BN, respectively. Atoms involved in the B_{1g} and B_{2u} modes vibrate along the [100] direction, atoms involved in the A_g and B_{3u} modes vibrate along the [010] direction, and atoms involved in the B_{2g} and B_{1u} modes vibrate along the [001] direction.

Figure 5(a) presents the calculated phonon band structure of Mo_2BC along the high symmetry directions in the Brillouin zone of base-centered orthorhombic lattice. Solid lines and blue circles show the phonon frequencies obtained from $(4 \times 4 \times 4)$ $\boldsymbol{q}$-point and $(3 \times 3 \times 3)$ $\boldsymbol{q}$-point meshes, respectively. The significant differences between these results indicate that the $(4 \times 4 \times 4)$ $\boldsymbol{q}$-point mesh is required for the calculation of phonon band structure. The phonon spectrum of Mo_2BC can be divided into two apparent regions with each of them including 12 phonon branches. The value of phonon bandgap between these two regions is around 2.33 THz. This gap is a consequence of the significant mass difference between Mo and B (C), which mainly leads to decoupling of molybdenum and boron (carbon) vibrations. The nature of the phonon band structure can be understood more clearly by analyzing the total and partial phonon DOS presented in Fig. 5(b). The heavier molybdenum atoms mainly contribute to the lower frequency phonon modes. In particular, the low-frequency phonon modes, below 5.5 THz, mainly originate from the second molybdenum (Mo2) atom, while the first molybdenum (Mo1) atom dominates the low-frequency phonon modes between 5.5 and 8.5 THz. These results imply that all three acoustic phonon modes arise mainly from the motion of the second molybdenum (Mo2) atom since they disperse up to around 5.0 THz. In the second frequency region of phonon DOS, the contributions of boron and carbon atoms are dominant because their masses are much lighter than that of molybdenum atoms. In particular, the sharp peak at around 20.3 THz is mainly formed by the vibrations of carbon atoms, while the last peak at around 22.9 THz is totally created by the vibrations of boron atoms. Obviously, this distribution of phonon modes for each atom is coherent with their atomic mass.

Figure 6(a) displays the calculated phonon band structure of Nb_2BN. Solid lines and blue circles show the phonon frequencies obtained from $(4 \times 4 \times 4)$ $\boldsymbol{q}$-point and $(3 \times 3 \times 3)$ $\boldsymbol{q}$-point meshes, respectively. The considerable differences between these results indicate that the $(4 \times 4 \times 4)$ $\boldsymbol{q}$-point mesh is also required for the

TABLE III. The estimated values of isotropic bulk modulus B_{VRH}, shear modulus G_{VRH}, Young's modulus E (all in GPa), B_H/G_H ratio, and Poisson's ratio (σ) for orthorhombic superconductors Mo_2BC and Nb_2BN.

Superconductor	B_V	B_R	B_H	G_V	G_R	G_H	E	B_H/G_H	σ
Mo_2BC	315.70	315.58	315.64	184.74	178.24	181.54	456.98	1.738	0.259
Experimental[29]							460		
GGA[29]	324	324	324	188	185	187	470	1.732	0.26
GGA[30]			313			181	455	1.730	
GGA[31]	334.0	332.4	333.2	200.4	193.2	196.8	494.2	1.690	0.253
Nb_2BN	284.10	283.88	283.99	184.71	177.56	181.14	448.11	1.568	0.236
GGA[31]	282.6	282.5	282.65	183.5	180.9	182.2	449.9	1.550	0.235

TABLE IV. Frequencies (ν in THz), electron–phonon coupling parameters (λ), and eigen characters of zone-center optical phonon modes for Mo_2BC. The notations of I and R correspond to infrared active and Raman active modes, respectively. Related atoms in B_{1g} and B_{2u} vibrate along the [100] direction, whereas contributing atoms in A_g and B_{3u} vibrate along the [010] direction. Furthermore, related atoms in B_{2g} and B_{1u} vibrate along the [001] direction.

Mode	ν	λ	Eigen characters	Mode	ν	λ	Eigen characters
B_{1g} (R)	4.377	0.308	**Mo2**+C	B_{2u}(I)	4.459	0.002	Mo1+Mo2+B+C
B_{1u} (I)	4.529	0.007	Mo1+Mo2+B+C	B_{2g}(R)	4.596	0.096	Mo1+**Mo2**+C
B_{1g} (R)	5.389	0.081	**Mo1**+B	A_g(R)	5.859	0.201	**Mo2**
B_{3u} (I)	6.651	0.011	Mo1+Mo2+B	B_{2g}(R)	6.986	0.062	**Mo1**+Mo2+B+C
A_g (R)	7.875	0.267	**Mo1**+B+C	B_{2u}(I)	10.991	0.001	**C**
B_{1u} (I)	11.182	0.004	**C**	B_{3u}(I)	13.921	0.006	**B**
B_{1g} (R)	14.517	0.103	B+**C**	B_{1u}(I)	14.774	0.001	**B**
B_{2g} (R)	14.983	0.097	**C**	B_{1g}(R)	16.819	0.026	**B**+C
B_{2u} (I)	17.334	0.002	**B**	A_g(R)	17.334	0.089	**B**
B_{3u} (I)	19.575	0.005	**C**	A_g(R)	20.205	0.087	**C**
B_{2g} (R)	22.788	0.017	**B**				

calculation of phonon band structure for Nb_2BN. Different from Mo_2BC, the phonon frequencies for this superconductor are separated into three distinct regions by two phonon bandgaps of 2.34 and 0.15 THz because of the mass difference between different types of atoms. All three acoustic phonon branches and nine optical phonon branches form a low-frequency region (LFR) below 8.83 THz, while six optical phonon branches are present in an intermediate-frequency region (IFR) between 11.17 and 15.88 THz. In addition to these regions, a high-frequency region (HFR) extends from 16.03 to 21.87 THz. It is worth emphasizing that all phonon branches in these regions display a large amount of dispersion. The character of all 24 phonon branches can be understood much better by examining the total and partial DOS presented in Fig. 6(b). Analyzing the partial phonon DOS, one can observe that, as expected, niobium the heaviest element dominates strongly the LFR. In particular, the lower part of this region (below 6.2 THz) is dominated by the vibrations of second Nb (Nb2) atoms, while dominance of the upper part is due to first Nb (Nb1) vibrations. The vibrations of boron and nitrogen atoms dominate the IFR and HFR. The contribution of nitrogen atoms is largest in the IFR. However, in a large part of this region, a strong N-B hybridization exists due to their similar masses. In the HFR, the vibrations of boron atoms are dominant but the sharpest peak at around 17.2 THz is almost totally formed by the vibrations of nitrogen atoms. Once again, this distribution of phonon modes is compatible with the atomic masses.

One of the main purposes of this work is to identify the most effective electron orbitals and phonon modes in developing superconductivity in these compounds. For this purpose, the Eliashberg spectral function $[\alpha^2F(\omega)]$ and the frequency variation of the total electron–phonon coupling parameter for Mo_2BC and Nb_2BN are illustrated in Figs. 7 and 8, respectively. An analysis of this function for Mo_2BC reveals that the phonon modes with low frequency (below 5.5 THz) offer almost 65% (0.484) to λ. This huge contribution can be linked to the factor $\frac{1}{\omega}$ in the integral formula of Eq. (3). According to this formula, their contribution to λ becomes larger because of their low frequency. This huge contribution means that these phonon modes couple strongly to electrons at the Fermi level.

TABLE V. Frequencies (ν in THz), electron–phonon coupling parameters (λ) and eigen characters of zone-center optical phonon modes for Nb_2BN. The notations of I and R correspond to infrared active and Raman active modes, respectively. Related atoms in B_{1g} and B_{2u} vibrate along the [100] direction, whereas contributing atoms to in A_g and B_{3u} vibrate along the [010] direction. Furthermore, related atoms in B_{2g} and B_{1u} vibrate along the [001] direction.

Mode	ν	λ	Eigen characters	Mode	ν	λ	Eigen characters
B_{2g} (R)	4.318	0.133	Nb1+**Nb2**+B+N	B_{1g}(R)	4.399	0.117	Nb1+Nb2+N
B_{1u} (I)	4.612	0.067	Nb1+Nb2+B+N	B_{2u}(I)	4.612	0.019	Nb1+Nb2+B+N
A_g (R)	6.145	0.508	Nb1+**Nb2**+B	B_{2g}(R)	6.785	0.113	**Nb1**+Nb2+B
B_{1g} (R)	6.881	0.123	**Nb1**+Nb2+B+N	B_{3u}(I)	7.012	0.006	Nb1+Nb2+B
A_g (R)	8.588	0.268	**Nb1**+Nb2+N	B_{2u}(I)	11.176	0.007	Nb2+**N**
B_{1u} (I)	11.658	0.002	Nb2+**N**	B_{1g}(R)	12.678	0.042	**N**
B_{2g} (R)	13.069	0.033	**N**	B_{3u}(I)	14.104	0.009	**B**
B_{1u} (I)	15.085	0.003	**B**	A_g(R)	16.766	0.279	B+N
B_{3u} (I)	17.439	0.003	**N**	B_{1g}(R)	17.505	0.052	**B**
A_g (R)	17.604	0.104	B+N	B_{2u}(I)	17.609	0.002	**B**
B_{2g} (R)	20.946	0.067	**B**				

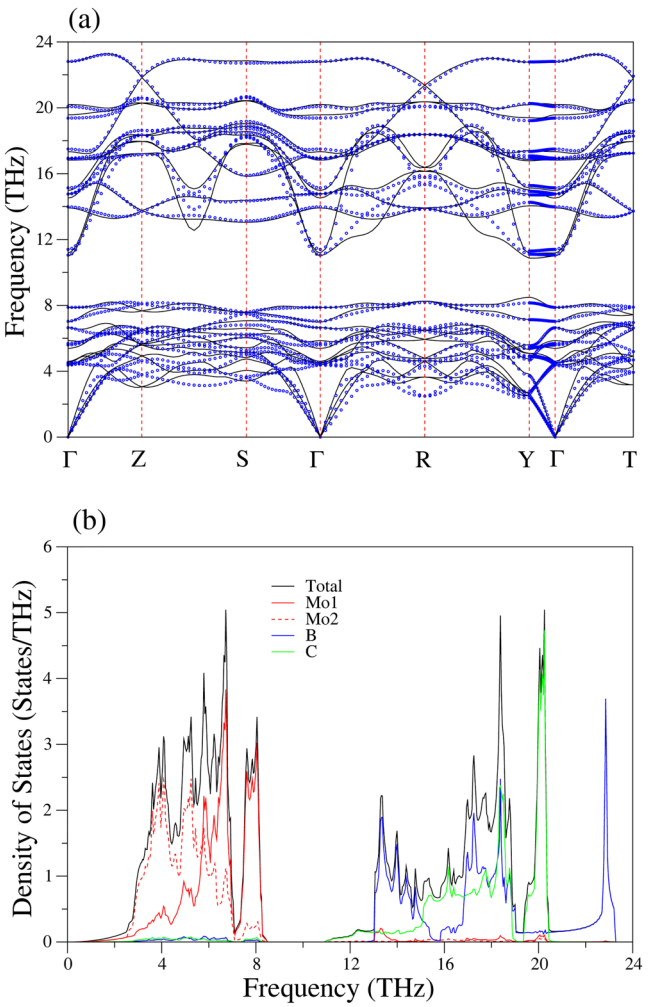

FIG. 5. (a) The calculated phonon band structure of Mo_2BC along the most important axes of symmetry in the Brillouin zone of base-centered orthorhombic lattice. Solid lines and blue circles show the phonon frequencies obtained from $(4 \times 4 \times 4)$ ***q***-point and $(3 \times 3 \times 3)$ ***q***-point meshes, respectively. The differences between these results indicate that the $(4 \times 4 \times 4)$ ***q***-point mesh is required for the calculation of phonon band structure. (b) Total and partial phonon density of states for Mo_2BC by using the $(4 \times 4 \times 4)$ ***q***-point mesh.

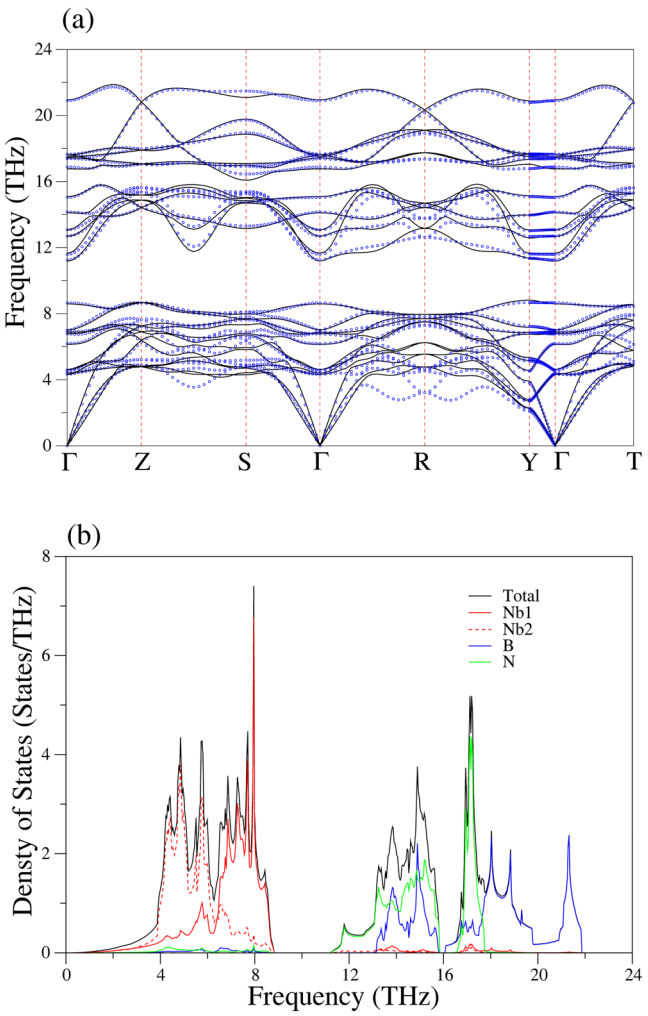

FIG. 6. (a) The calculated phonon band structure of Nb_2BN along the most important axes of symmetry in the Brillouin zone of base-centered orthorhombic lattice. Solid lines and blue circles show the phonon frequencies obtained from $(4 \times 4 \times 4)$ ***q***-point and $(3 \times 3 \times 3)$ ***q***-point meshes, respectively. The differences between these results indicate that the $(4 \times 4 \times 4)$ ***q***-point mesh is required for the calculation of phonon band structure. (b) Total and partial phonon density of states for Nb_2BN by using the $(4 \times 4 \times 4)$ ***q***-point mesh.

This strong coupling is expected because the corresponding phonon modes mainly imply second molybdenum (Mo2) atoms, which dominate the electronic states near the Fermi level with their d states. In addition to this huge contribution, the Mo1-related phonon modes contribute in the order of 22% to λ. The remaining 13% of λ is contributed by the vibrations of nonmetal atoms. This small contribution signals that their vibrations are very weakly involved in the process of scattering electrons because of the insignificant existence of their p states at the Fermi level.

In agreement with Mo_2BC, transition metal-related vibrations are strongly involved in the process of scattering electrons, while the vibrations of nonmetal atoms play a relatively insignificant role in determining the superconducting properties of Nb_2BN. We find that the total electron–phonon coupling is equal to 0.539 for Nb_2BN, being smaller than the corresponding value of 0.745 for Mo_2BC. This difference must be the main reason why Mo_2BC has a higher T_c value than its isostructural compound Nb_2BN because a higher value of λ indicates a higher value of T_c. As a consequence, the T_c difference between Mo_2BC and Nb_2BN can be explained in terms of their $N(E_F)$ and λ values.

The calculated values of $N(E_F)$, ω_{ln}, λ, T_c, and γ for both investigated superconductors are presented in Table VI, together with the

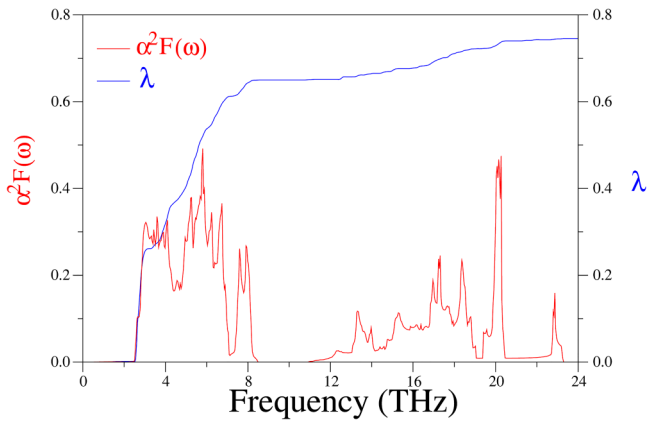

FIG. 7. The Eliashberg spectral function $\alpha^2F(\omega)$ (red lines) and the frequency dependence of average electron–phonon coupling parameter λ (blue lines) for Mo_2BC.

existing experimental results[21,22,26,27] and previous GGA results.[27,31] In general, our calculated parameters for both studied compounds harmonize very well with the existing experimental[21,22,26,27] and theoretical results.[27,31] In particular, the electron–phonon coupling parameter is calculated to be 0.745 and 0.539 for Mo_2BC and Nb_2BN, respectively. These values are comparable with their experimental values of 0.75 and 0.62.[26,27] When the $\mu^\star$ value is taken as 0.13, the value of superconducting transition temperature is found to be 7.41 K for Mo_2BC and 3.50 K for Nb_2BN. The calculated T_c value of Mo_2BC is in good agreement with its experimental value of 7.2,[27] while the calculated T_c value of Nb_2BN lies between the experimental values of 4.4 and 2.5 K.[26,28] As mentioned before, $\mu^\star$ generally takes values between 0.10 and 0.20.[39–41,49] The calculated T_c value is 9.41 K for $\mu^\star = 0.10$ and 3.54 K for $\mu^\star = 0.20$ for Mo_2BC. The average of these limiting values is 6.48 K, which is still comparable

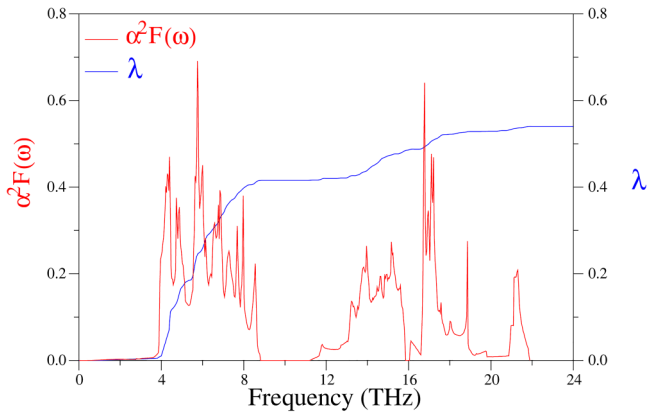

FIG. 8. The Eliashberg spectral function $\alpha^2F(\omega)$ (red lines) and the frequency dependence of average electron–phonon coupling parameter λ (blue lines) for Nb_2BN.

TABLE VI. The calculated values of physical quantities associated with superconductivity in Mo_2BC and Nb_2BN. Available experimental data and previous theoretical results are also included for comparison.

Phase	N(E_F) [states/(eV atom)]	ω_{ln} (K)	λ	T_c (K)	γ ($\frac{mJ}{mol\,K^2}$)
Mo_2BC	2.909	233.587	0.745	7.41	5.97
Experimental[21]				7.0–5.3	
Experimental[22]				6.33	
Experimental[27]			0.75	7.2	
GGA[31]	2.872				
GGA[27]	3.060				
Nb_2BN	2.325	333.190	0.539	3.50	4.21
Experimental[26]			0.62	4.4	6.3
Experimental[28]				2.5	
GGA[31]	2.302				2.73

with the experimental value of 7.2 K.[27] For the same limiting values of $\mu^\star$, the values of T_c are found to be 5.39 and 0.78 K for Nb_2BN, respectively. Once again, their average value of 3.09 K still lies between the corresponding experimental values of 4.4 and 2.5 K.[26,28] Furthermore, the calculated value of 4.21 $\frac{mJ}{mol\,K^2}$ for γ using the approximate expression in Eq. (6) for Nb_2BN is more comparable with its experimental value of 6.3 $\frac{mJ}{mol\,K^2}$[26] than its previous GGA value of 2.73 $\frac{mJ}{mol\,K^2}$.[31] The Sommerfeld coefficient (γ) gives a vague idea of the electronic specific heat at low temperatures. The γ value gives us the main idea that the compound has a weak or strong correlation. Low values indicate agreement with the BCS theory, while high values may mean that it contains heavy-Fermionic features. In this case, the compound has an unconventional superconducting property. When the electron–boson interaction passes the strong coupling limit, the temperature-dependent formula must be used instead of low temperature (see Ref. 49). The error margin between experimental and theoretical values has not had much meaning for this parameter (as in Ref. 30) since it gives a small idea of electronic correlation. The low value of γ tells us that the compounds have a weak electronic correlation. In addition to the N(E_F) and λ values of Mo_2BC being higher than those of Nb_2BC, the ω_{ln} value of the former is lower than that of the latter. We could have expected this result because the softening of ω_{ln} for Mo_2BC has the potential to increase its λ value according to the McMillan–Hopfield expression [see Eq. (7)]. For this reason, the value of T_c for Mo_2BC becomes higher than that for Nb_2BN because of the larger electron–phonon coupling parameter of the former as compared to that of the latter.

IV. SUMMARY

In this paper, we have conducted *ab initio* pseudopotential calculations in order to understand the structural, electronic, elastic, mechanical, phononic, and electron–phonon interaction properties of Mo_2BC and Nb_2BN superconductors. It is argued that the chemical bonding in these compounds is a mixed one, arising out of ionic, covalent, and metallic characters. The near-Fermi electronic states of both superconductors are occupied by the d states of transition metal atoms, but the electronic density of

states at the Fermi level in Mo_2BC is significantly higher than that in Nb_2BN. The considerable difference in their $N(E_F)$ values is the first reason why Mo_2BC has a higher T_c value than its isostructural compound Nb_2BN, since a higher value of $N(E_F)$ gives rise to a higher electron–phonon coupling parameter (λ).

Both compounds are stable according to the criteria of mechanical stability. The bulk modulus, shear modulus, and Young's modulus for Mo_2BC are larger than the corresponding values for Nb_2BN, revealing the stronger borocarbide stiffness. Adopting the ductility and brittleness in terms of the limiting value of 1.75 for the ratio of the bulk modulus to the shear modulus, our work suggests that Mo_2BC is moderately inclined to ductility, while Nb_2BN is considerably inclined to brittleness.

The phonon frequency spectrum of Mo_2BC shows a broad gap between approximately 8.51 THz and approximately 10.84 THz for Mo_2BC. The phonon frequency spectrum of Nb_2BN shows a broad gap between approximately 8.83 THz and approximately 11.17 THz and a small gap between approximately 15.88 THz and approximately 16.03 THz. Analysis of phonon density of states for both superconductors reveals dominance of transition metal atoms in the low-frequency region and dominance of lighter nonmetal atoms in the high-frequency region.

The calculated Eliashberg spectral functions indicate that transition metal-related vibrations are strongly involved in the process of scattering electrons, while the vibrations of nonmetal atoms play a relatively insignificant role in determining the superconducting properties due to the absence of their p states at the Fermi level. We find that the total electron–phonon coupling is equal to 0.745 for Mo_2BC, being larger than the corresponding value of 0.539 for Nb_2BN. The difference in the λ values must be the second reason why Mo_2BC has a higher T_c value than its isostructural compound Nb_2BN. Finally, we find that the superconducting transition temperature is equal to 7.41 K for Mo_2BC and 3.50 K for Nb_2BN, being comparable with their experimental values of 7.2 and 4.4 K. As a consequence, we can conclude that the conventional electron–phonon coupling theory conveniently describes superconductivity in both Mo_2BC and Nb_2BN.

ACKNOWLEDGMENTS

Numerical calculations were performed using the Intel Nehalem (i7) cluster (ceres) at the University of Exeter.

DATA AVAILABILITY

The data that support the findings of this study are available from the corresponding author upon reasonable request.

REFERENCES

[1]J. G. Chen, "Carbide and nitride overlayers on early transition metal surfaces: Preparation, characterization, and reactivities," Chem. Rev. **96**, 1477 (1996).
[2]J. G. Chen, J. Eng, and S. P. Kelty, "NEXAFS determination of electronic and catalytic properties of transition metal carbides and nitrides: From single crystal surfaces to powder catalysts," Catal. Today **43**, 147 (1998).
[3]Y. Kumashiro, *Electric Refractory Materials* (Marcel Dekker, New York, 2000).
[4]J. A. Nelson and M. J. Wagner, "High surface area Mo_2C and WC prepared by alkalide reduction," Chem. Mater. **14**, 1639 (2002).
[5]H. H. H. Wu and J. G. Chen, "Surface chemistry of transition metal carbides," Chem. Rev. **105**, 185 (2005).
[6]J. B. Levine, S. H. Tolbert, and R. B. Kaner, Adv. Funct. Mater. **19**, 3519 (2009).
[7]A. Friedrich, B. Winkler, E. A. Juarez-Arellano, and L. Bayarjargal, "Synthesis of binary transition nitrides, carbides and borides from the elements in the laser heated diamond anvil cell and their structure-property relations," Materials **4**, 1648 (2011).
[8]L. E. Toth, *Transition Metal Carbides and Nitrides* (Academic Press, New York, 1971).
[9]V. A. Gubanov, A. L. Ivanovsky, and V. P. Zhukov, *Electronic Structure of Refractory Carbides and Nitrides* (Cambridge University Press, Cambridge, 1994).
[10]J. C. Crowhurst, A. F. Goncharov, B. Sadigh, C. L. Evans, P. G. Morrall, J. L. Ferreira, and A. J. Nelson, Science **311**, 1275 (2006).
[11]A. F. Young, C. Sanloup, E. Gregoryanz, S. Scandolo, R. J. Hemley, and H. Mao, Phys. Rev. Lett. **96**, 155501 (2006).
[12]H. Y. Chung, M. B. Weinberger, J. B. Levine, A. Kavner, J. M. Yang, S. H. Tolbert, and R. B. Kaner, Science **316**, 436 (2007).
[13]M. Wiefssner, M. Leisch, H. Emminger, and A. Kulmburg, "Phase transformation study of a high speed steel powder by high temperature X-ray diffraction," Mater. Charact. **59**, 937 (2008).
[14]X. H. Wang, F. Han, X. M. Liu, S. Y. Qu, and Z. D. Zou, "Effect of molybdenum on the microstructure and wear resistance of Fe-based hardfacing coatings," Mater. Sci. Eng., A **489**, 193 (2008).
[15]A. S. Chaus and M. Hudakova, "Wear resistance of high-speed steels and cutting performance of tool related to structural factors," Wear **267**, 1051 (2009).
[16]H. J. Fink, A. C. Thorsen, E. Parker, V. F. Zackay, and L. Toth, "High-field superconductivity of carbides," Phys. Rev. **138**, A1170 (1965).
[17]V. Sadagapan and H. C. Gatos, "Superconductivity in the transition metal carbides: $Mo_{4.8}Si_3C_{0.6}$, $Mo_{0.95}Hf_{0.05}C_{0.75}$ and Mo_2C," J. Phys. Chem. Solids **27**, 235 (1966).
[18]L. E. Toth, C. M. Yen, L. G. Rosneb, and D. E. Anderson, "Superconducting critical fields, currents and temperatures in the Nb-Zr-N ternary system," J. Phys. Chem. Solids **27**, 1815 (1966).
[19]K. Hechler, E. Saur, and H. Wizgall, "Critical data of niobium nitride in transverse magnetic fields," Z. Phys. **205**, 400 (1967).
[20]C. M. Yen, L. E. Toth, Y. M. Shy, D. E. Anderson, and L. G. Rosner, "Superconducting H_c-J_c and T_c measurements in the Nb–Ti–N, Nb–Hf–N, and Nb–V–N ternary systems," J. Appl. Phys. **38**, 2268 (1967).
[21]L. E. Toth, "High superconducting transition temperatures in the molybdenum carbide family of compounds," J. Less-Common Met. **13**, 129 (1967).
[22]L. E. Toth and J. Zbasnik, "Low temperature heat capacities of superconducting molybdenum carbides," Acta Metall. **16**, 1177 (1968).
[23]G. S. Smith, A. G. Tharp, and Q. Johnson, "Determination of the light-atom positions in Mo_2BC," Acta Crystallogr. B **25**, 698 (1969).
[24]J.-O. Bovin, M. O'Keeffe, and L. Stenberg, "Planar defects in Mo_2BC. An electron microscope study," J. Solid State Chem. **22**, 221 (1977).
[25]C. P. Poole Jr., *Handbook of Superconductivity*, 1st ed. (Academic Press, San Diego, 2000), Chap. 6, p. 142.
[26]O. V. Cigarroa, S. T. Renosto, and A. J. S. Machado, "Conventional superconductivity properties of the ternary boron-nitride Nb_2BN," Supercond. Sci. Technol. **27**, 035005 (2014).
[27]R. Escamilla, E. Carvajal, M. Cruz-Irisson, F. Morales, L. Huerta, and E. Verdin, "XPS study of the electronic density of states in the superconducting Mo_2B and Mo_2BC compound," J. Mater. Sci. **51**, 6411 (2016).
[28]P. Rogl, H. Klesnar, and P. Fisher, "Neutron powder diffraction of Nb_2BN_{1-x}," J. Am. Ceram. Soc. **71**, C450–C452 (1988).
[29]J. Emmerlich, D. Music, M. Braun, P. Fayek, F. Munnik, and J. M. Schneider, "A proposal for an unusually stiff and moderately ductile hard coating material: Mo_2BC," J. Phys. D: Appl. Phys. **42**, 185406 (2009).
[30]H. Bolvardi, J. Emmerlich, M. Baben, D. Music, J. von Appen, R. Dronskowski, and J. M. Schneider, "Systematic study on the electronic structure and mechanical properties of X_2BC (X = Mo, Ti, V, Zr, Nb, Hf, Ta and W)," J. Phys.: Condens. Matter **25**, 045501 (2013).

[31]D. V. Suetin and I. R. Shein, "Electronic and mechanical properties, phase stability, and formation energies of point defects of niobium boronitride Nb_2BN," Phys. Solid State **59**, 1481 (2017).
[32]P. Giannozzi, S. Baroni, N. Bonini, M. Calandra, R. Car, C. Cavazzoni, D. Ceresoli, G. L. Chiarotti, M. Cococcioni, I. Dabo, A. Dal Corso, S. de Gironcoli, S. Fabris, G. Fratesi, R. Gebauer, U. Gerstmann, C. Gougoussis, A. Kokalj, M. Lazzeri, L. Martin-Samos, N. Marzari, F. Mauri, R. Mazzarello, S. Paolini, A. Pasquarello, L. Paulatto, C. Sbraccia, S. Scandolo, G. Sclauzero, A. P. Seitsonen, A. Smogunov, P. Umari, and R. M. Wentzcovitch, "QUANTUM ESPRESSO: A modular and open-source software project for quantum simulations of materials," J. Phys.: Condens. Matter **21**, 395502 (2009).
[33]P. Giannozzi, O. Andreussi, T. Brumme, O. Bunau, M. Buongiorno Nardelli, M. Calandra, R. Car, C. Cavazzoni, D. Ceresoli, M. Cococcioni, N. Colonna, I. Carnimeo, A. Dal Corso, S. de Gironcoli, P. Delugas, R. A. DiStasio, Jr., A. Ferretti, A. Floris, G. Fratesi, G. Fugallo, R. Gebauer, U. Gerstmann, F. Giustino, T. Gorni, J. Jia, M. Kawamura, H.-Y. Ko, A. Kokalj, E. Küçükbenli, M. Lazzeri, M. Marsili, N. Marzari, F. Mauri, N. L. Nguyen, H.-V. Nguyen, A. Otero-de-la-Roza, L. Paulatto, S. Poncé, D. Rocca, R. Sabatini, B. Santra, M. Schlipf, A. P. Seitsonen, A. Smogunov, I. Timrov, T. Thonhauser, P. Umari, N. Vast, X. Wu, and S. Baroni, "Advanced capabilities for materials modelling with quantum ESPRESSO," J. Phys.: Condens. Matter **29**, 465901 (2017).
[34]A. Dal Corso, "Elastic constants of beryllium: A first-principles investigation," J. Phys.: Condens. Matter **28**, 075401 (2016).
[35]W. Voigt, *Lehrbuch der Kristallphysik* (Taubner, Leipzig, 1928).
[36]A. Reuss, "Berechnung der fließgrenze von mischkristallen auf grund der plastizitätsbedingung für einkristalle," Z. Angew. Math. Mech. **9**, 49 (1929).
[37]R. Hill, "The elastic behaviour of a crystalline aggregate," Proc. Phys. Soc. Sect., A **65**, 349 (1952).
[38]Z.-J. Wu, E.-J. Zhao, H.-P. Xiang, X.-F. Hao, X.-J. Liu, and J. Meng, "Crystal structures and elastic properties of superhard IrN_2 and IrN_3 from first principles," Phys. Rev. B **76**, 054115 (2007).
[39]W. L. McMillan, "Transition temperature of strong-coupled superconductors," Phys. Rev. **167**, 331 (1968).
[40]P. B. Allen and R. C. Dynes, "Transition temperature of strong-coupled superconductors reanalyzed," Phys. Rev. B **12**, 905 (1975).
[41]P. B. Allen and R. C. Dynes, "Superconductivity at very strong coupling," J. Phys. C: Solid State Phys. **8**, L158 (1975).
[42]W. Kohn and L. J. Sham, "Self-consistent equations including exchange and correlation effects," Phys. Rev. **140**, A1133 (1965).
[43]J. P. Perdew, K. Burke, and M. Ernzerhof, "Generalized gradient approximation made simple," Phys. Rev. Lett. **77**, 3865 (1996).
[44]D. Vanderbilt, "Soft self-consistent pseudopotentials in a generalized eigenvalue formalism," Phys. Rev. B **41**, 7892R (1990).
[45]T. H. Fischer and J. Almlof, "General methods for geometry and wave function optimization," J. Phys. Chem. **96**, 9768 (1992).
[46]H. J. Monkhorst and J. D. Pack, "Special points for Brillouin-zone integrations," Phys. Rev. B **13**, 5188 (1976).
[47]A. B. Migdal, "Interaction between electrons and lattice vibrations in a normal metal," Zh. Eksp. Teor. Fiz. **34**, 996 (1958); available at http://www.w2agz.com/Library/Classic%20Papers%20in%20Superconductivity/Migdal,%20Strong%20e-p%20Interactions,%20Sov-Phys%20JETP%206,%20996%20(1958).pdf.
[48]G. M. Eliashberg, "Interaction between electrons and lattice vibrations in a superconductor," Sov. Phys. JETP **11**, 696 (1960); available at http://www.w2agz.com/Library/Classic%20Papers%20in%20Superconductivity/Eliashberg,%20e-p%20Interactions%20in%20SCs,%20Sov-Phys%20JETP%2011,%20696%20(1960).pdf.
[49]A. P. Durajski, R. Szczesniak, Y. Li, C. Wang, and J.-H. Cho, "Isotope effect in superconducting lanthanum hydride under high compression," Phys. Rev. B **101**, 214501 (2020).
[50]J. P. Carbotte, "Properties of boson-exchange superconductors," Rev. Mod. Phys. **62**, 1027 (1990).
[51]F. D. Murnaghan, "The compressibility of media under extreme pressures," Proc. Natl. Acad. Sci. U.S.A. **50**, 697 (1944).
[52]K. Chen, L. R. Zhao, J. Rodgers, and J. S. Tse, "Alloying effects on elastic properties of TiN-based nitrides," J. Phys. D: Appl. Phys. **36**, 2725 (2003).
[53]H. Yao, L. Ouyang, and W.-Y. Ching, "*Ab initio* calculation of elastic constants of ceramic crystals," J. Am. Ceram. Soc. **90**, 3194 (2007).
[54]V. Krasnenko and M. G. Brik, "First-principles calculations of hydrostatic pressure effects on the structural, elastic and thermodynamic properties of cubic monocarbides," Solid State Sci. **14**, 1431 (2012).
[55]A. Kokalj, "XCrySDen—A new program for displaying crystalline structures and electron densities," J. Mol. Graph. Model. **17**(3-4), 176–179 (1999).
[56]S. F. Pugh, "XCII. Relations between the elastic moduli and the plastic properties of polycrystalline pure metals," Philos. Mag. **45**, 823 (1954).
[57]J. Haines, J. M. Leger, and G. Bocquillon, "Synthesis and design of superhard materials," Annu. Rev. Mater. Res. **31**, 1 (2001).